

Multiscale Crystal Plasticity Modeling Considering Nucleation of Dislocations Based on Thermal Activation Process on Ultrafine-grained Aluminum

Y Aoyagi

Department of Finemechanics, Tohoku University
6-6-01 Aoba, Aramaki, Aoba-ku, Sendai, 980-8579, JAPAN

aoyagi@tohoku.ac.jp

Abstract. In this study, a crystal plasticity model expressing the behavior of the dislocation source and the mobile dislocations is proposed by considering a thermal activation process of dislocations. In order to predict the variation of critical resolved shear stress due to grain boundaries, mobile dislocations, or dislocation sources, information on these crystal defects is introduced into a hardening law of crystal plasticity. The crystal orientation and shape of ultrafine-grained (UFG) aluminum produced by accumulative roll bonding processes are measured by electron backscatter diffraction (EBSD). Mechanical properties of the UFG aluminum are estimated using tensile test and indentation test. Results obtained by EBSD are introduced into a computational model. Finite element simulation for polycrystal of aluminum investigates the effect of microstructure on mechanical properties of UFG aluminum.

1. Introduction

High-strength, light-weight metal materials are required to improve safety and reduce transportation cost. Ultrafine-grained (UFG) metals produced by severe plastic deformation have attracted interest as high-strength materials [1]-[4]. UFG metals with a grain size of less than 1 μ m exhibit remarkable mechanical properties (e.g., increased yield stress, decreased hardening ratio, yield point drop of FCC metal [5], temperature dependency [6], tension-compression asymmetry [7], and increased strain-rate sensitivity [8]). A computational model predicting these properties is desired in the field of materials science and engineering. Multiscale crystal plasticity models expressing a size effect on grain size have been proposed by introducing information on grain size as a material parameter [9], [10]. However, conventional theory cannot express the effect of the dislocation source and the grain boundary precisely and directly. It is assumed that such unusual mechanical properties originate from the exhaustion of dislocation sources and the enormous volume fraction of the grain boundary. Recently, the effect of the grain boundary has attracted the attention of many researchers as an important factor determining the mechanical properties of UFG metal [11]-[15].

In this study, a crystal plasticity model expressing the behavior of the dislocation source and the mobile dislocations is proposed by considering a thermal activation process of dislocations. In order to predict the variation of critical resolved shear stress due to grain boundaries, mobile dislocations, or dislocation sources, information on these crystal defects is introduced into a hardening law of crystal plasticity. The crystal orientation and shape of UFG aluminum produced by accumulative roll bonding (ARB) processes are measured by electron backscatter diffraction (EBSD). Mechanical properties of the UFG aluminum are estimated using tensile and indentation tests. Using results obtained by EBSD,



information on crystal orientation and shape are introduced into a computational model for multiscale crystal plasticity simulation. Finite element simulation for polycrystal of aluminum investigates the effects of dislocation behavior and crystal orientation on mechanical properties of UFG aluminum.

2. Multiscale crystal plasticity model

In previous work, we defined the flow stress of crystal plasticity considering information on dislocations and grain boundaries, which are dislocation sources [16]. Since the work hardening caused by accumulation of dislocations and the generation of dislocations should alternatively occur, the flow stress of this model is modified as

$$g^{(\alpha)} = \max\{\tau_d^{(\alpha)}, \min(\tau_s^{(\alpha)}, \tau_m^{(\alpha)})\} \quad (1)$$

where $g^{(\alpha)}$ is flow stress on the slip system α , $\tau_d^{(\alpha)}$ is the deformation resistance originating in accumulated dislocations, $\tau_s^{(\alpha)}$ is that originating in the initial dislocation sources, and $\tau_m^{(\alpha)}$ is that originating in mobile dislocations. Equation (1) indicates that plastic deformation is caused by activation of the dislocation source that is most easily activated. Usually, $\tau_d^{(\alpha)}$ is given by the extended Bailey-Hirsch equation [17]. Frequency on thermal activation process a at a dislocation segment is given by

$$p_a = \frac{N_a}{N_r} \nu \exp\left\{\frac{-\Delta G_a(1-\tau/\tau_a)}{k_B T}\right\} \quad (2)$$

where $N_a = \rho_a / \tilde{b}$ is the number of dislocation segments, N_r is the reference value of N_a , ν is the atomic frequency, ΔG_a is the thermal activation energy, τ is the applied shear stress, τ_a is the reference stress on the process a , k_B is the Boltzmann constant, and T is the temperature. When $p_a = 1$, $\tau_s^{(\alpha)}$ and $\tau_m^{(\alpha)}$ are obtained as

$$\tau_s^{(\alpha)} = \tau_{FR} - \frac{k_B T}{\tilde{b}^3} \ln \frac{\rho_s^{(\alpha)}}{\tilde{b}} \frac{\nu}{N_r}, \quad \tau_m^{(\alpha)} = \tau_{MD} - \frac{k_B T}{\tilde{b}^3} \ln \frac{\rho_{gn}^{(\alpha)}}{\tilde{b}} \frac{\nu}{N_r} \quad (3)$$

where τ_{FR} is the resolved shear stress when dislocation loops are released from a Frank-Read (F-R) source, \tilde{b} is the magnitude of the Burgers vector, $\rho_s^{(\alpha)}$ is the density of the dislocation source, $\tau_{MD}^{(\alpha)}$ is the resolved shear stress when the mobile dislocations move, and $\rho_{gn}^{(\alpha)}$ is the mobile dislocation density. The variables in equation (3) are given by

$$\rho_s^{(\alpha)} = \rho_{s0}^{(\alpha)} + e(\rho_d^{(\alpha)} - \rho_0^{(\alpha)}), \quad \rho_{gn}^{(\alpha)} = \|\rho_{gn}^{(\alpha)}\| = \|(\mathbf{s}^{(\alpha)} \otimes \mathbf{m}^{(\alpha)}) \times \nabla \gamma^{(\alpha)} / \tilde{b}\|, \\ \tau_{MD}^{(\alpha)} = (\tau_{GT} + \tau_{PN}) / 2 - (\tau_{GT} - \tau_{PN}) \tanh\left\{c(\phi_g^{(\alpha)} - \phi_r) / \phi_r\right\} / 2, \quad \phi_g^{(\alpha)} = |\text{curl} \mathbf{m}^{(\alpha)}| \quad (4)$$

where $\rho_{s0}^{(\alpha)}$ is the initial density of dislocation sources, e is the ratio of the dislocation density on dislocation sources and the others, $\rho_d^{(\beta)}$ is the dislocation density, $\rho_0^{(\alpha)}$ is the initial dislocation density, $\rho_{gn}^{(\alpha)}$ is the geometrically necessary (GN) dislocation density tensor [17], $\mathbf{s}^{(\alpha)}$ is the slip direction vector, $\mathbf{m}^{(\alpha)}$ is the normal direction of the slip plane, $\gamma^{(\alpha)}$ is the slip, τ_{GT} is the resolved shear stress when the mobile dislocations across grain boundary, τ_{PN} is the critical shear stress based on the Peierls-Nabarro stress, $\phi_g^{(\alpha)}$ is the misorientation parameter, and ϕ_r is the threshold of misorientation. Equation (3) represents the local increase of CRSS in a region without a dislocation source or a mobile dislocation. It is reported that thermal activation of the F-R sources hardly affects some mechanical properties of UFG metals [18]. Under the situation assumed in this paper, the value of τ is about the same as or larger than that of τ_a . Therefore, the influence of the thermal activation process on activation of the F-R source is extremely small. Equation (3)₁ is modeled to express information on the decrease in the frequency of plastic deformation due to exhaustion of dislocation sources, i.e. the change of $\tau_s^{(\alpha)}$ depending on the density of dislocation source. An elasto-viscoplastic constitutive equation for a crystal plasticity model, the hardening modulus representing the interaction of slip systems, and the definition of dislocation density are same as the previous model [16]. The rate of dislocation density $\dot{\rho}_d^{(\beta)}$ is given by

$$\dot{\rho}_d^{(\beta)} = (1 - k \rho_d^{(\beta)}) r \rho_f |\dot{\gamma}^{(\beta)}| / \tilde{b}, \quad (5)$$

where k is the annihilation ratio and corresponds to the inverse of the saturated density of dislocation, r is the mean length of the remaining dislocation lines, and ρ_f is the density of forest dislocations.

3. Methods of measuring and properties of UFG material

3.1. Experiment Procedures

Ultrafine-graining using the ARB process [3] is performed for industrial pure aluminum JIS-A1050. In this study, a 2 mm-thick aluminum sheet is rolled to 1 mm thickness at room temperature. A UFG aluminum is produced by eight cycles of ARB. The material after eight cycles of ARB is not annealed. We treat unrolled specimens that are annealed for 1 h at 673 K as a starting material. The grain size and crystal orientation of specimens made from the starting and the UFG materials are estimated using EBSD from the transverse direction (TD) that is perpendicular to the normal direction (ND) and the rolling direction (RD). Mechanical properties of these materials are measured by tensile tests with a universal testing machine. The tensile direction coincides with the RD. The thickness of specimens for the starting materials is 2 mm and that for the UFG materials is 1 mm, and the gage length for the UFG material is 12 mm, and the width is 5 mm. Micro indentation tests using a spherical indenter are performed for the UFG specimen after 0.0%, 0.5%, 1.0%, 1.5%, 2.0%, and 2.5% tension in order to investigate the effect of pre-strain on the mechanical properties of the UFG material. The radius of the indenter is 50 μm . The indenter is forced into the surface of the specimen from the ND. The maximum load is 0.8826 N, the forcing time is 10 s, the force duration is 1 s, and the unloading time is 10 s.

3.2. Experiment Results for the Starting and UFG Materials

Figures 1 and 2 depict the distribution of crystal orientation and the $\langle 111 \rangle$ pole figure of the starting and UFG materials measured using EBSD. The color map depicted in these figures is hereinafter used

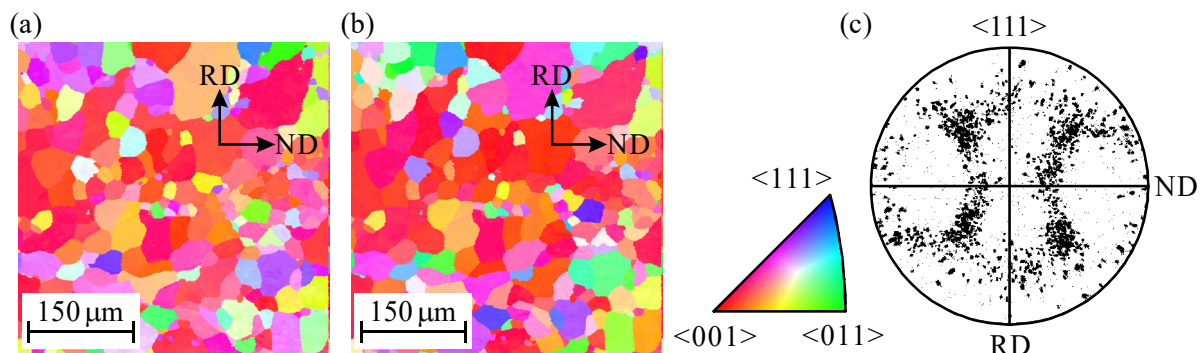


Figure 1. Crystal orientation for (a) ND and (b) RD, (c) the $\langle 111 \rangle$ pole figure for the starting material measured using EBSD.

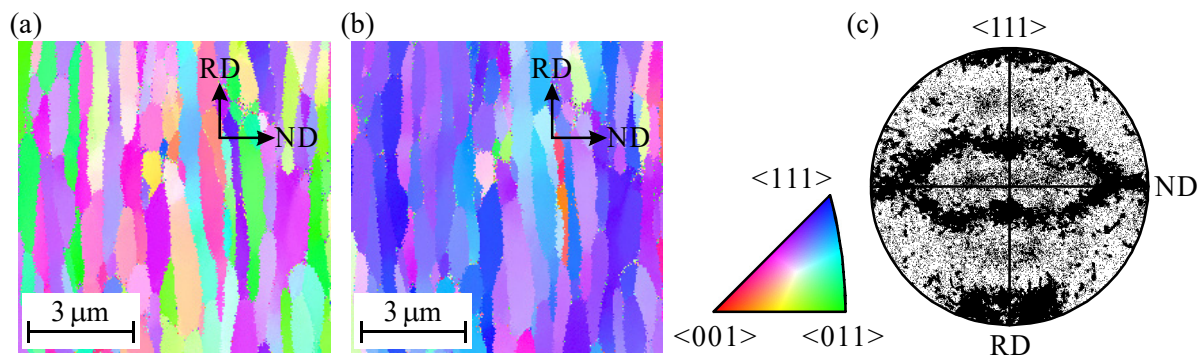


Figure 2. Crystal orientation for (a) ND and (b) RD, and (c) the $\langle 111 \rangle$ pole figure for the UFG material measured using EBSD.

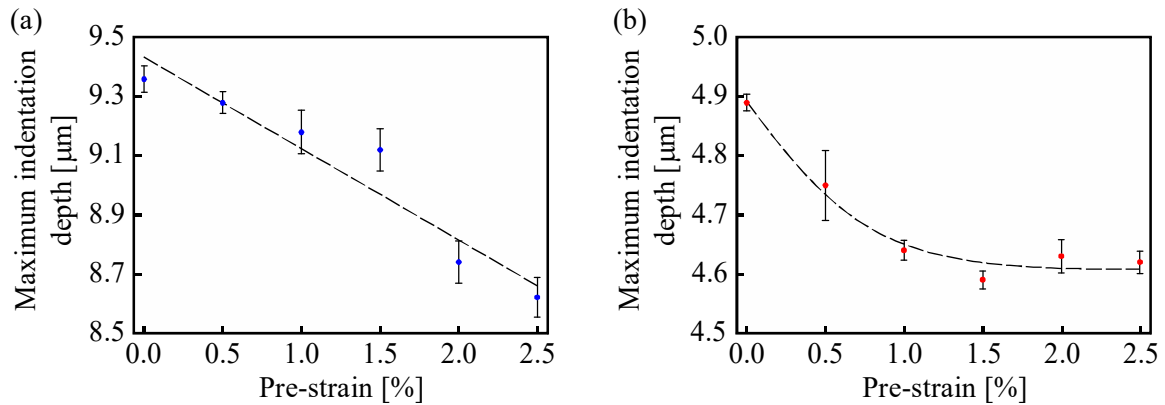


Figure 3. Maximum indentation depth for the starting (a) and UFG (b) materials.

for the color of crystal orientation. The mean grain size of the starting material along the ND is 30 μm , and that along the RD is 32 μm . In contrast, the mean grain size of the UFG material along the ND is 0.39 μm , and that along the RD is 1.8 μm . The rolling texture is developed by eight cycles of ARB. Figure 2 indicates that $\langle 111 \rangle$ directions tend to orient to the RD. Result obtained by the tensile tests are shown later with simulation results.

Figure 3 plots the maximum indentation depth measured by the micro indentation test for the pre-strained starting and UFG materials. The maximum indentation depth of the starting material decreases proportionally with the increase of pre-strain because of work-hardening by tensile deformation. The maximum indentation depth for the UFG material strengthened by the ARB process is less than that of the starting material and approaches the fixed value after 1.0% pre-strain. This result indicates that dislocation density is saturated after 1.0% pre-strain, and the work-hardening ratio decreases.

4. Pseudo three-dimensional simulation of aluminum

4.1. Numerical Procedures

FE method is applied for the present crystal plasticity analysis. Figures 4 and 5 depict periodic unit-cell models used in this calculation. We conduct a pseudo three-dimensional computation, which restricts the three-dimensional plastic deformation of metal to two-dimensional components on an observation plane [16]. In the present simulation, a polycrystal of aluminum under plane stress is assumed, and we control displacement at the overlapping vertexes depicted by black dots in figures 4(a) and 5(a), so that the volume mean of the stress component xx becomes zero, and tensile displacement in the RD is applied at the upper vertexes of the specimen. The aspect ratio of grains is 1 for the starting material or 5 for the UFG material. The initial crystal orientations of each grain, which are randomly selected from the results of EBSD, are depicted in figures 4 and 5. The red dots in figures 4(c) and 5(c) represent the $\langle 111 \rangle$ pole figures for the computational model.

The material constants and numerical parameters are the critical shear stress based on Peierls-Nabarro stress $\tau_{PN}=10\text{ MPa}$; the minimum shear stress when dislocations across grain boundaries $\tau_{GT}=300\text{ MPa}$; the threshold of misorientation $\phi_r=3\times 10^7$; the annihilation ratio $k=2\times 10^{-15}$; and the mean length of the remaining dislocation lines $r=4\text{ nm}$. In general, the shear stress when dislocation loops are released from the F-R source are given by $\tau_{FR}=\mu b/l$, where l is the distance between slip planes. The values of the total initial dislocation density ρ_{t0} is measurable physical quantities. However, it is difficult to estimate experimentally these values. Therefore, this value is determined by fitting a simulated stress-strain curve to the experiment curve. The size of the dislocation source for the starting material is one third the size of each grain (i.e., 10 μm), and that for the UFG material is 0.3 μm , which is slightly smaller than the mean grain size along the ND.

4.2. Numerical Results and Discussion

Figure 6 plots the nominal stress versus nominal strain curves with the experiment one for the starting

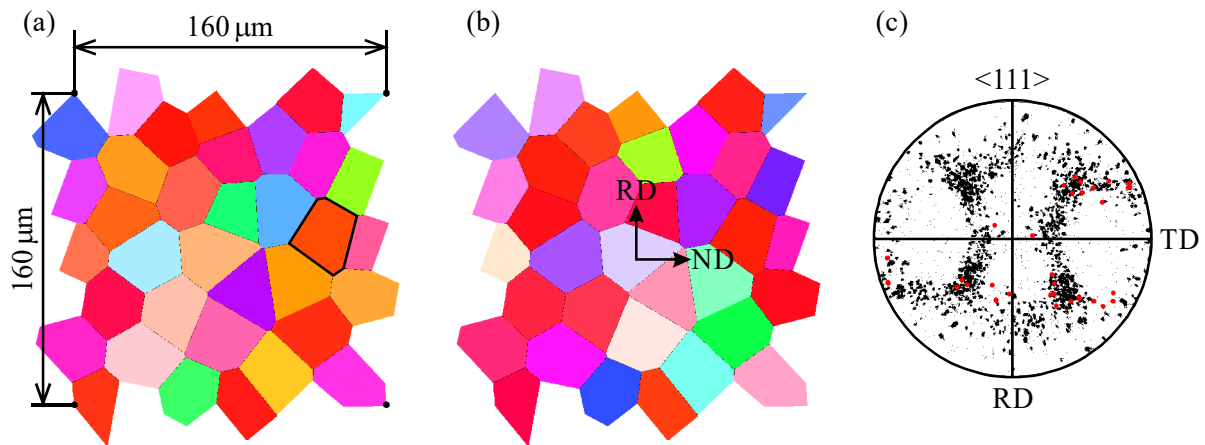


Figure 4. Crystal orientation in the ND (a), RD (b), and $\langle 111 \rangle$ pole figure for the starting material.

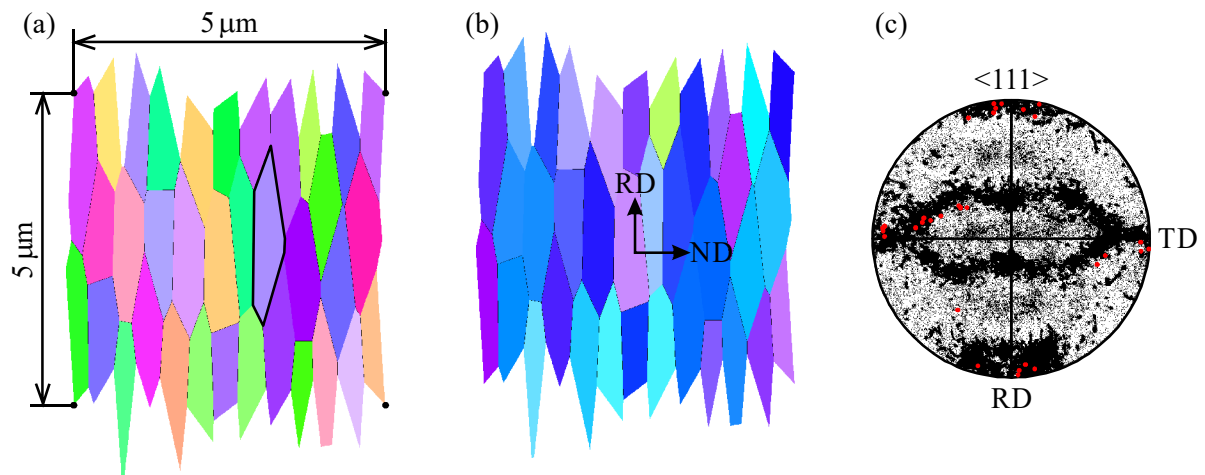


Figure 5. Crystal orientation in the ND (a), RD (b), and $\langle 111 \rangle$ pole figure for the UFG material (c).

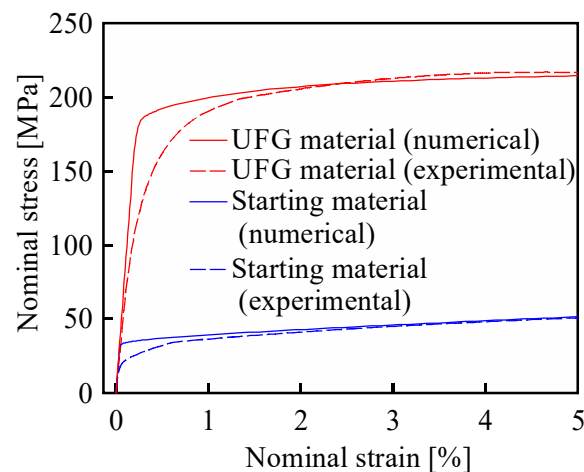


Figure 6. Nominal stress versus nominal strain curves for the starting and UFG materials calculated by the multiscale crystal plasticity model.

and UFG materials. The values of ρ_{t0} are determined as $3 \times 10^{12} \text{ m}^{-2}$ and $1 \times 10^{14} \text{ m}^{-2}$ for the starting and UFG materials by this simulation. General curves can be reproduced by adjustment of these values.

Figure 7 plots the mean dislocation density of the primary and secondary slip systems of a grain, denoted by bold lines in figures 4(a) and 5(a). The dislocation density of the starting material does not reach the saturated dislocation density at 5% elongation. The dislocation density of the primal slip

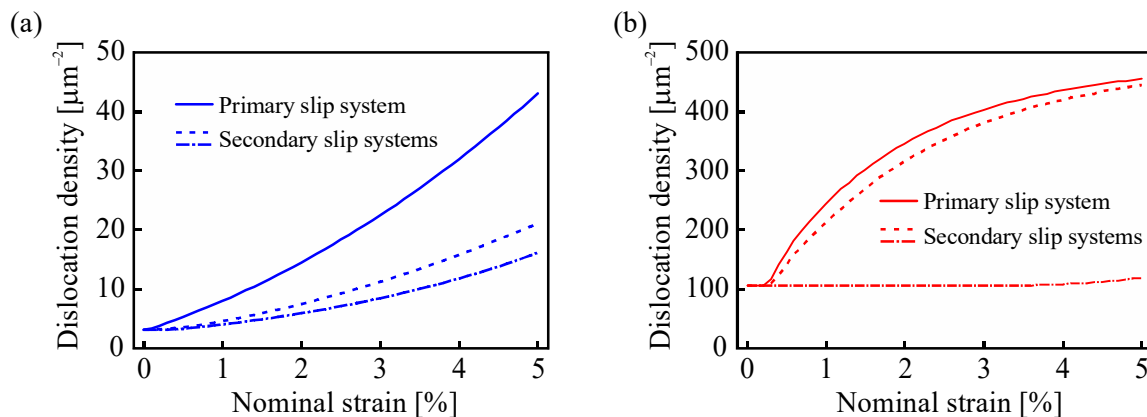


Figure 7. Dislocation density of the primary and secondary slip systems in a central grain of the specimen for the (a) starting and (b) UFG materials.

system for the UFG material approaches the saturated dislocation density at the early stage of deformation. Comparison of figures 3 and 7 indicates that the nominal strains at which the gradient of curve changes are similar. The simulation result agrees well with the experimental tendency [19] that the dislocation density of the starting material increases gradually after yielding and the increase rate of the dislocation density of the UFG material decreases with the decrease of the work-hardening ratio.

These results suggest that the work-hardening ratio becomes low when the dislocation density in the primary slip system is saturated. Since the decrease of work-hardening caused by saturation of dislocation density reduces ductility, total elongation for the UFG material becomes lower than for the starting material.

5. Conclusions

Fitting a stress-strain curve calculated by the multiscale crystal plasticity model to the experiment curve determines the initial dislocation density. The dislocation density of the UFG material is saturated in the early stage of tensile deformation, and the work-hardening ratio becomes low.

References

- [1] Horita Z, Smith D J, Furukawa M, Nemoto M, Valiev R Z and Langdon T G 1996 *J. Mater. Res.* **11** 1880
- [2] Belyakov A, Gao W, Miura H and Sakai T 1998 *Metall. Mater. Trans A* **29** 2957
- [3] Saito Y, Tsuji N, Utsunomiya H, Sakai T and Hong R G 1998 *Scr. Mater.* **39** 1221
- [4] Kim H-W, Kanga S-B, Tsuji N and Minamino Y 2005 *Acta Mater.* **53** 1737
- [5] Segal V M, Ferrasse S and Alford F 2006 *Mater. Sci. Eng. A* **422** 321
- [6] Duckham A, Zhang D Z, Liang D, Luzin V, Cammarata R C, Leheny R L, Chien C L and Weihs T P 2003 *Acta Mater.* **51** 4083
- [7] Cheng S, Spencer J A and Milligan W 2003 *Acta Mater.* **51** 4505
- [8] Sabirov I, Barnett M R, Estrin Y and Hodgson P D 2009 *Scripta Mater.* **61** 181
- [9] Ohashi T, Kawamukai M and Zbib H M 2007 *Int. J. Plasticity* **23** 897
- [10] Ohno N and Okumura D 2007 *J. Mech. Phys. Solids* **55** 1879
- [11] Lim H, Lee M G, Kim J H, Adams B L and Wagoner R H 2011 *Int. J. Plasticity* **27** 1328
- [12] Duhamel C, Brechet Y and Champion Y 2010 *Int. J. Plasticity* **26** 747
- [13] Lee M G, Lim H, Adams B L, Hirth J P and Wagoner R H 2010 *Int. J. Plasticity* **26** 925
- [14] Liu Z L, Zhuang Z, Liu X M, Zhao X C and Zhang Z H 2011 *Int. J. Plasticity* **27** 201
- [15] Aoyagi Y, Kobayashi R, Kaji Y and Shizawa K 2013 *Int. J. Plasticity* **47** 13
- [16] Aoyagi Y, Tsuru T and Shimokawa T 2014 *Int. J. Plasticity* **55** 43
- [17] Aoyagi Y and Shizawa K 2007 *Int. J. Plasticity* **23** 1022
- [18] Estrin Y, Kim H S and Nabarro F R N 2007 *Acta Mater.* **55** 6401
- [19] Adachi H, Miyajima Y, Sato M and Tsuji N 2014 *J. Jpn. Inst. Light Met.* **64** 463 (Japanese)